

## Detection schemes for quantum vacuum diffraction and birefringence

N. Ahmadiiaz<sup>1</sup>, T. E. Cowan<sup>1,2</sup>, J. Grenzer<sup>1</sup>, S. Franchino-Viñas<sup>1</sup>, A. Laso Garcia<sup>1</sup>,  
M. Šmíd<sup>1</sup>, T. Toncian<sup>1</sup>, M. A. Trejo<sup>1</sup>, and R. Schützhold<sup>1,3</sup>

<sup>1</sup>*Helmholtz-Zentrum Dresden-Rossendorf, Bautzner Landstraße 400, 01328 Dresden, Germany*

<sup>2</sup>*Institut für Kern- und Teilchenphysik, Technische Universität Dresden, 01062 Dresden, Germany*

<sup>3</sup>*Institut für Theoretische Physik, Technische Universität Dresden, 01062 Dresden, Germany*



(Received 26 April 2023; accepted 15 September 2023; published 10 October 2023)

Motivated by recent experimental initiatives, such as at the Helmholtz International Beam line for Extreme Fields at the European X-ray Free Electron Laser, we calculate the birefringent scattering of x rays at the combined field of two optical (or near-optical) lasers and compare various scenarios. In order to facilitate an experimental detection of quantum vacuum diffraction and birefringence, special emphasis is placed on scenarios where the difference between the initial and final x-ray photons is maximized. Apart from their polarization, these signal and background photons may differ in propagation direction (corresponding to scattering angles in the millirad regime) and possibly energy.

DOI: [10.1103/PhysRevD.108.076005](https://doi.org/10.1103/PhysRevD.108.076005)

### I. INTRODUCTION

The quantum vacuum is not just empty space—as the ground state of interacting quantum field theories, it displays a complex structure, entailing many fascinating phenomena. For example, quantum electrodynamics (QED) predicts that the quantum vacuum should behave like a nonlinear medium and, thus, display effects such as diffraction and refraction as well as birefringence under the influence of a strong electromagnetic field [1–5].

Related phenomena have already been observed in the form of Delbrück scattering of  $\gamma$  rays on the Coulomb fields of nuclei, which can be interpreted as quantum vacuum refraction [6–16], or the interaction of the Coulomb fields of two nuclei almost colliding with each other at ultrahigh energies and the resulting emission of a pair of  $\gamma$  quanta [17,18].

In contrast, we are mostly interested in scenarios without additional massive particles (such as nuclei; see also [19]) and at subcritical scales in the following: First, the relevant energies and momenta should be well below the electron mass  $m \approx 0.51 \text{ MeV}/c^2$  and, thus, the characteristic length and timescales well above the reduced Compton length  $\lambda = \hbar/(mc) \approx 386 \text{ fm}$ . Second, the involved field strengths should be well below the critical fields of QED, i.e.,  $E_{\text{crit}} = m^2 c^3 / (\hbar q) \approx 1.3 \times 10^{18} \text{ V/m}$  as well as  $B_{\text{crit}} = E_{\text{crit}}/c \approx 4.4 \times 10^9 \text{ T}$ .

Many theoretical and several experimental investigations have been devoted to this subcritical regime. For polarizing the quantum vacuum, one could use a strong and quasistatic magnetic field [20–29] or the focus of an optical or near-optical laser or x-ray free electron laser (XFEL) as the pump field; see, e.g., [30–51]. For the detection of the induced vacuum nonlinearity, one could also employ an

optical or near-optical laser or an XFEL as the probe field; see, e.g., [19,30–38]. Motivated by experimental facilities such as the Helmholtz International Beam line for Extreme Fields (HIBEF) and the quest to maximize the signal, we consider an XFEL probe (whose shorter wavelength yields a larger interaction probability in a given volume) and an optical pump field (which facilitates a high intensity).

In spite of the efforts so far, neither quantum vacuum birefringence [52] nor quantum vacuum diffraction—or, more generally, quantum vacuum nonlinearity in the subcritical regime—have been conclusively verified in a laboratory experiment yet [25–27]. Apart from a pure verification of this fundamental QED prediction, such an experiment would also allow us to search for new phenomena beyond the standard model of particle physics, because they could manifest themselves in measurable deviations from the QED predictions.

In order to facilitate such an experiment, it is crucial to distinguish the signal (consisting of one or a few x-ray photons) from the background, i.e., the XFEL pulse. Since such a distinction purely based on the photon polarizations can be quite challenging, it has been suggested to consider scenarios where the initial (background) and final (signal) x-ray photons also differ in propagation direction and possibly energy; see, e.g., [40,53]. Developing these ideas further, we propose and study scenarios (see Fig. 1) which maximize this difference, especially the momentum transfer and, thus, the scattering angle.

### II. EFFECTIVE LAGRANGIAN

Since all the involved scales are supposed to be subcritical, we start from the generalized lowest-order Euler-Heisenberg Lagrangian ( $\hbar = c = \epsilon_0 = \mu_0 = 1$ ):

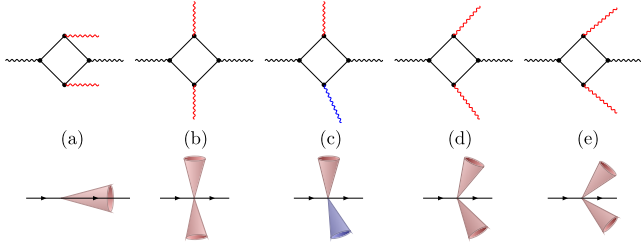


FIG. 1. Sketch of the counterpropagating (a), crossed-beam (b), five-o'clock (c), five-past-five (d), and ten-past-four (e) scenarios (from left to right). In the bottom row, the XFEL photons are depicted as horizontal black lines, while the focused optical lasers are represented by red ( $\omega = 1.5$  eV) or blue ( $\omega = 3$  eV) cones. The top row displays a typical Feynman diagram where the color coding and the angle indicate which beam the involved photon lines belong to.

$$\mathfrak{L} = \frac{1}{2}(\mathfrak{E}^2 - \mathfrak{B}^2) + a(\mathfrak{E}^2 - \mathfrak{B}^2)^2 + b(\mathfrak{E} \cdot \mathfrak{B})^2, \quad (1)$$

in terms of the total electric  $\mathfrak{E}$  and magnetic  $\mathfrak{B}$  fields. In QED, the two parameters  $a$  and  $b$  are given by  $b = 7a$  and  $a = q^4/(360\pi^2 m^4)$ ; for reviews, see Refs. [54–58]. However, in order to accommodate possible deviations from the standard model, we shall keep them as general. For example, a coupling to an axion field would typically manifest itself in a modification of the  $b$  parameter while  $a$  remains unchanged; see, e.g., [59–62].

The propagation of the probe field  $\mathbf{E}$  and  $\mathbf{B}$  (i.e., the XFEL) in the presence of a given pump field  $\mathbf{E}_L$  and  $\mathbf{B}_L$  (i.e., the optical laser) can be studied by inserting the split  $\mathfrak{E} = \mathbf{E}_L + \mathbf{E}$  and  $\mathfrak{B} = \mathbf{B}_L + \mathbf{B}$  and linearizing the equations of motion, leading to the effective Lagrangian

$$\mathfrak{L}_{\text{eff}} = \frac{1}{2}[\mathbf{E} \cdot (\mathbf{1} + \delta\epsilon) \cdot \mathbf{E} - \mathbf{B} \cdot (\mathbf{1} - \delta\mu) \cdot \mathbf{B}] + \mathbf{E} \cdot \delta\Psi \cdot \mathbf{B}, \quad (2)$$

with the symmetric permittivity and permeability tensors

$$\begin{aligned} \delta\epsilon^{ij} &= 8aE_L^i E_L^j + 2bB_L^i B_L^j + 4a\delta^{ij}(\mathbf{E}_L^2 - \mathbf{B}_L^2), \\ \delta\mu^{ij} &= 2bE_L^i E_L^j + 8aB_L^i B_L^j - 4a\delta^{ij}(\mathbf{E}_L^2 - \mathbf{B}_L^2), \end{aligned} \quad (3)$$

plus the symmetry-breaking contribution

$$\delta\Psi^{ij} = -8aE_L^i B_L^j + 2bB_L^i E_L^j + 2b\delta^{ij}(\mathbf{E}_L \cdot \mathbf{B}_L), \quad (4)$$

which describe the polarizability of the QED vacuum. Note that the latter tensor is not symmetric  $\delta\Psi^{ij} \neq \delta\Psi^{ji}$ .

As is well known, the linearized equations of motion generated by (2) can be cast into the same form as the macroscopic Maxwell equations in a medium  $\nabla \cdot \mathbf{D} = 0$ ,  $\nabla \cdot \mathbf{B} = 0$ ,  $\nabla \times \mathbf{E} = -\partial_t \mathbf{B}$ , and  $\nabla \times \mathbf{H} = \partial_t \mathbf{D}$ , provided that we introduce the electric  $\mathbf{D} = (\mathbf{1} + \delta\epsilon) \cdot \mathbf{E} + \delta\Psi \cdot \mathbf{B}$  and magnetic  $\mathbf{H} = (\mathbf{1} - \delta\mu) \cdot \mathbf{B} - \delta\Psi^T \cdot \mathbf{E}$  displacement fields.

### III. SCATTERING THEORY

The scattering of the x-ray photons can be calculated via various options, e.g., time-dependent perturbation theory of quantum fields or the photon emission picture (see, e.g., [46]). In the following, we shall employ classical scattering theory [19,32,63] but adapted to the case of oscillating contributions in  $\delta\epsilon$ ,  $\delta\mu$ , and  $\delta\Psi$ . To this end, we combine the above Maxwell equations to

$$\square \mathbf{D} = \nabla \times [\nabla \times (\mathbf{D} - \mathbf{E})] + \partial_t [\nabla \times (\mathbf{H} - \mathbf{B})] = \mathbf{J}^{\text{eff}}, \quad (5)$$

where the effective source term  $\mathbf{J}^{\text{eff}}$  on the right-hand side encodes the quantum vacuum nonlinearity (see Appendix B for its explicit expression). Since this term is very small, we may employ the usual Born approximation. Thus, we split the XFEL field  $\mathbf{D}$  into an ingoing plane wave  $\mathbf{D}^{\text{in}}$  with  $\omega_{\text{in}}$  and  $\mathbf{k}_{\text{in}}$  plus a small scattering contribution  $\mathbf{D}^{\text{out}}$  induced by vacuum polarizability  $\delta\epsilon$ ,  $\delta\mu$ , and  $\delta\Psi$ .

These quantities  $\delta\epsilon$ ,  $\delta\mu$ , and  $\delta\Psi$  depend on the optical laser (i.e., pump) fields  $\mathbf{E}_L$  and  $\mathbf{B}_L$  and, thus, on time. Here, we assume that this pump field is generated by the superposition of two optical lasers, i.e.,  $\mathbf{E}_L = \mathbf{E}_1 + \mathbf{E}_2$  and  $\mathbf{B}_L = \mathbf{B}_1 + \mathbf{B}_2$  which oscillate with frequencies  $\omega_1$  and  $\omega_2$ , respectively. Because of the resulting oscillatory time dependence of  $\delta\epsilon$ ,  $\delta\mu$ , and  $\delta\Psi$ , the outgoing field  $\mathbf{D}^{\text{out}}$  contains various frequency contributions  $\omega_{\text{out}} = \omega_{\text{in}} \pm \omega_1 \pm \omega_2$  (similar to Floquet bands). Since the combinations  $\omega_{\text{out}} = \omega_{\text{in}} + \omega_1 + \omega_2$  and  $\omega_{\text{out}} = \omega_{\text{in}} - \omega_1 - \omega_2$  are typically not allowed by energy-momentum conservation (see below), we focus on  $\omega_{\text{out}} = \omega_{\text{in}} + \omega_1 - \omega_2$  and  $\omega_{\text{out}} = \omega_{\text{in}} - \omega_1 + \omega_2$  in the following.

Then, in the frequency domain, Eq. (5) turns into a Helmholtz equation (more details are included in Appendix B):

$$\square \mathbf{D}_{\omega}^{\text{out}} = -(\nabla^2 + \omega_{\text{out}}^2) \mathbf{D}_{\omega}^{\text{out}} = \mathbf{J}_{\omega}^{\text{eff}}, \quad (6)$$

which can be solved by the usual Greens function. In the far field, we thus obtain the scattering amplitude

$$\mathfrak{A} = \frac{1}{4\pi |\mathbf{D}_{\omega}^{\text{in}}|} \mathbf{e}_{\text{out}} \cdot \int d^3r \exp\{-i\mathbf{k}_{\text{out}} \cdot \mathbf{r}\} \mathbf{J}_{\omega}^{\text{eff}}, \quad (7)$$

depending on the momentum  $\mathbf{k}_{\text{out}}$  and polarization  $\mathbf{e}_{\text{out}}$  of the outgoing x-ray photon. Since  $\omega_1$  and  $\omega_2$  are optical or near-optical frequencies of the order of  $\mathcal{O}(\text{eV})$  while  $\omega_{\text{out}}$  and  $\omega_{\text{in}}$  are x-ray frequencies on the keV regime, we may neglect small terms such as  $\omega_1/\omega_{\text{out}}$  (in comparison to a nonvanishing leading-order term) in the following and approximate  $\omega_{\text{out}} \approx \omega_{\text{in}}$ .

Furthermore, the integral in Eq. (7) simplifies drastically if we approximate the two optical (pump) lasers by plane waves with momenta  $\mathbf{k}_1$  and  $\mathbf{k}_2$  and polarizations  $\mathbf{e}_1$  and  $\mathbf{e}_2$ . In this case, the  $d^3r$  integral just corresponds to

momentum conservation, and the scattering amplitude simplifies to

$$\mathfrak{A} \approx 2\pi^2 \mathfrak{F} E_1 E_2 \omega_{\text{out}}^2 \delta^3(\mathbf{k}_{\text{out}} - \mathbf{k}_{\text{in}} - \mathbf{k}_1 + \mathbf{k}_2), \quad (8)$$

where  $\mathfrak{F}(\mathbf{e}_1, \mathbf{e}_2, \mathbf{e}_{\text{in}}, \mathbf{e}_{\text{out}}, \mathbf{n}_1, \mathbf{n}_2, \mathbf{n}_{\text{in}}, \mathbf{n}_{\text{out}})$  is a purely algebraic expression of the four polarization vectors  $\mathbf{e}_I$  and propagation direction unit vectors  $\mathbf{n}_I = \mathbf{k}_I/\omega_I$ .

In order to obtain a compact expression for  $\mathfrak{F}$ , we will make explicit use of its symmetry under permutations of the indices in the kinematical variables; we will, thus, write a single contribution, and permutations thereof should be added. Using this convention,  $\mathfrak{F}$  is given as

$$\mathfrak{F} = a\mathfrak{F}_a + b\mathfrak{F}_b, \quad (9)$$

where we have defined

$$\begin{aligned} \mathfrak{F}_a &= [(\mathbf{e}_2 \cdot \mathbf{e}_{\text{in}}) - (\mathbf{e}_2 \times \mathbf{n}_2) \cdot (\mathbf{e}_{\text{in}} \times \mathbf{n}_{\text{in}})] \\ &\quad \times [(\mathbf{e}_{\text{out}} \times \mathbf{n}_{\text{out}}) \cdot (\mathbf{e}_1 \times [\mathbf{n}_{\text{out}} - \mathbf{n}_1])] \\ &\quad + \text{permutations}\{1, 2, \text{in}\}, \\ \mathfrak{F}_b &= \frac{1}{2} [(\mathbf{n}_{\text{out}} \times (\mathbf{e}_1 \times \mathbf{n}_1) - \mathbf{e}_1) \times \mathbf{n}_{\text{out}}] \cdot \mathbf{e}_{\text{out}} \\ &\quad \times [\mathbf{e}_2 \cdot (\mathbf{e}_{\text{in}} \times \mathbf{n}_{\text{in}})] + \text{permutations}\{1, 2, \text{in}\}. \end{aligned} \quad (10)$$

As explained above, we have to sum over permutations; i.e., for each expression  $\mathfrak{F}_{a,b}\{1, 2, \text{in}\}$ , we have to add the other five combinations  $\mathfrak{F}_{a,b}\{1, \text{in}, 2\}$ ,  $\mathfrak{F}_{a,b}\{2, \text{in}, 1\}$ ,  $\mathfrak{F}_{a,b}\{2, 1, \text{in}\}$ ,  $\mathfrak{F}_{a,b}\{\text{in}, 1, 2\}$ , and  $\mathfrak{F}_{a,b}\{\text{in}, 2, 1\}$ .

#### IV. COUNTERPROPAGATING CASE

Let us first consider the setup already discussed in the literature [31,35], where the XFEL interacts with a single counterpropagating optical laser; see Fig. 1(a). In this case, the two pump beams coincide and form a single optical laser which is counterpropagating to the XFEL. Thus, we set  $\omega_1 = \omega_2$  and  $\mathbf{e}_1 = \mathbf{e}_2$  as well as  $\mathbf{n}_1 = \mathbf{n}_2$ , which implies  $\omega_{\text{out}} = \omega_{\text{in}}$  and  $\mathbf{n}_{\text{in}} = \mathbf{n}_{\text{out}}$ . Hence, we have  $\mathbf{n}_{\text{in}} = \mathbf{n}_{\text{out}} = -\mathbf{n}_1 = -\mathbf{n}_2$ , and  $\mathfrak{F}$  simplifies to

$$\begin{aligned} \mathfrak{F} &= 16a(\mathbf{e}_{\text{in}} \cdot \mathbf{e}_1)(\mathbf{e}_{\text{out}} \cdot \mathbf{e}_1) \\ &\quad + 4b\mathbf{e}_{\text{in}} \cdot (\mathbf{n}_{\text{in}} \times \mathbf{e}_1)\mathbf{e}_{\text{out}} \cdot (\mathbf{n}_{\text{in}} \times \mathbf{e}_1). \end{aligned} \quad (11)$$

For the polarization-conserving signal  $\mathbf{e}_{\text{in}} = \mathbf{e}_{\text{out}}$ , this simplifies to  $\mathfrak{F}_{\parallel} = 16a(\mathbf{e}_{\text{in}} \cdot \mathbf{e}_1)^2 + 4b[\mathbf{e}_{\text{in}} \cdot (\mathbf{n}_{\text{in}} \times \mathbf{e}_1)]^2$ . If all polarizations are aligned  $\mathbf{e}_{\text{in}} = \mathbf{e}_1$ , the  $a$  term in Eq. (1) contributes. In contrast, the  $b$  term corresponds to an interaction between the electric component of the XFEL and the magnetic component of the optical laser and vice versa. These two orientations  $\mathbf{e}_{\text{in}} = \mathbf{e}_1$  and  $\mathbf{e}_{\text{in}} \perp \mathbf{e}_1$  correspond to the major axes of the refractive index [52]. For initial photon polarizations in between, we also get

birefringent scattering  $\mathbf{e}_{\text{in}} \perp \mathbf{e}_{\text{out}}$  with the amplitude  $\mathfrak{F}_{\perp}$ . For example, for an orientation at  $45^\circ$ , we find  $\mathfrak{F}_{\perp} = 8a - 2b$ . As expected, the birefringent amplitude  $\mathfrak{F}_{\perp}$  scales with the difference of the eigenvalues of the refractive index along its two major axes [52].

In the purely counterpropagating case, the energy-momentum transfer is exactly zero; i.e., the scattering angle vanishes. Thus, the signal and background photons can be distinguished only by their polarization, which is an experimental challenge. A finite (albeit small) scattering angle can be induced by the spatial inhomogeneity of laser focus (i.e., going beyond the plane-wave approximation), in close analogy to a lens (quantum vacuum refraction); see also [44,48].

#### V. CROSSED-BEAM CASE

##### A. Plane-wave approximation

The above difficulty can be avoided by considering a modified scenario where the pump field is generated by two optical laser beams with the same frequency  $\omega_1 = \omega_2$  and field strength but different propagation directions  $\mathbf{n}_1 \neq \mathbf{n}_2$ . In Ref. [40], a fully perpendicular setup with  $\mathbf{n}_1 \perp \mathbf{n}_2$  has been considered. However, in order to maximize the momentum transfer (i.e., have a large scattering angle), we propose the head-on collision of two optical laser beams where  $\mathbf{n}_1 = -\mathbf{n}_2$ . This momentum transfer does also mark the primary distinction to Ref. [32] where an analogous setup has been considered but focusing on forward scattering. Since the XFEL beam mainly jitters in horizontal direction, the crossed-beam geometry has the advantage of being quite robust if the optical lasers are also oriented in horizontal direction.

Here, we consider the case  $\mathbf{e}_1 = \mathbf{e}_2$  which yields the maximum electric pump field but other polarizations (e.g., maximum magnetic field) would work as well. Since  $\omega_1 = \omega_2$ , the energy transfer vanishes again  $\omega_{\text{out}} = \omega_{\text{in}}$ , but we get a finite momentum transfer  $\Delta\mathbf{k} = 2\omega_1\mathbf{n}_1$ . In order to satisfy  $\omega_{\text{out}} = \omega_{\text{in}}$  and to transform this momentum transfer into a maximum scattering angle (in the millirad regime), we assume sending in the probe beam at a perpendicular direction  $\mathbf{n}_{\text{in}} \perp \mathbf{n}_1$  and  $\mathbf{n}_{\text{in}} \perp \mathbf{e}_1$ ; see Fig. 1(b). In this case, we find

$$\mathfrak{F} = 4a(\mathbf{e}_{\text{in}} \cdot \mathbf{e}_1)(\mathbf{e}_{\text{out}} \cdot \mathbf{e}_1) + b(\mathbf{e}_{\text{in}} \cdot \mathbf{n}_1)(\mathbf{e}_{\text{out}} \cdot \mathbf{n}_1). \quad (12)$$

The polarization-conserving signals  $\mathfrak{F}_{\parallel}^{\uparrow} = 4a$  for the case  $\mathbf{e}_{\text{in}} = \mathbf{e}_{\text{out}} = \mathbf{e}_1$  and  $\mathfrak{F}_{\parallel}^{\leftrightarrow} = b$  for the case  $\mathbf{e}_{\text{in}} = \mathbf{e}_{\text{out}} = \mathbf{n}_1$  (i.e., along the major axes of the refractive index [52]) would allow us to detect the parameters  $a$  and  $b$  separately. As before, we also get birefringent scattering  $\mathbf{e}_{\text{in}} \perp \mathbf{e}_{\text{out}}$  in the other directions; e.g.,  $\mathfrak{F}_{\perp} = 2a - b/2$  for the orientation at  $45^\circ$ .

Note that the polarization conserving signals can also be distinguished from the background by the momentum

transfer yielding a scattering angle in the millirad regime. This scattering angle can be explained in close analogy to diffraction (as in ordinary Bragg scattering). The spatial modulation (in the  $\mathbf{n}_1$  direction) acts like a grating which generates a Bragg peak at  $\Delta\mathbf{k} = 2\omega_1\mathbf{n}_1$ .

### B. Cross section for a real pulse

The amplitude (7) yields the differential cross section  $d\sigma/d\Omega = |\mathfrak{A}|^2$ . Obviously, inserting the plane-wave result (8), this quantity would diverge due to the infinite volume. Thus, let us consider the more realistic case of a finite-size laser focus. To estimate the cross section, we rewrite the amplitude (7) by factoring out the frequency, wave number, and amplitude of the XFEL; summing the amplitudes from all the available processes as described in Appendix B, we obtain

$$\mathfrak{A} = \frac{\omega_{\text{out}}^2}{4\pi} \int d^3r \exp\{i\Delta\mathbf{k} \cdot \mathbf{r}\} j^{\text{eff}}, \quad (13)$$

where  $\Delta\mathbf{k} = \mathbf{k}_{\text{in}} - \mathbf{k}_{\text{out}}$  is the momentum transfer. The renormalized source term  $j^{\text{eff}}(\mathbf{r})$  now depends on only the optical laser and the XFEL polarization vectors. For example, for the case  $\mathbf{e}_{\text{in}} = \mathbf{e}_{\text{out}} = \mathbf{e}_1$  discussed above, we find  $j^{\text{eff}}(\mathbf{r}) = 8a\langle\mathbf{E}_L^2(t, \mathbf{r})\rangle = 8a\langle[\mathbf{E}_1(t, \mathbf{r}) + \mathbf{E}_2(t, \mathbf{r})]^2\rangle$ , where  $\langle\cdots\rangle$  denotes the temporal average (in a first approximation, the time dependence of the *in* and *out* fields counterbalance each other).

Now let us assume that the spatial dependence of  $j^{\text{eff}}(\mathbf{r})$  along the XFEL beam direction can be approximated (at least well inside the Rayleigh length) by a simple (e.g., Gaussian) envelope function  $f(r_{\parallel})$  such that  $j^{\text{eff}}(\mathbf{r}) = f(r_{\parallel})j_{\perp}^{\text{eff}}(\mathbf{r}_{\perp})$ . Furthermore, in view of energy conservation and  $\omega_{\text{in}} = \omega_{\text{out}} \gg \omega_1 = \omega_2$ , the momentum transfer  $\Delta\mathbf{k}$  is approximately perpendicular to  $\mathbf{k}_{\text{in}}$ . Thus, we may approximate the integral over the solid angle  $\int d\Omega$  by an integration over the transversal momentum transfer  $\int d\Omega \approx \omega_{\text{out}}^{-2} \int d^2\Delta\mathbf{k}_{\perp}$ . This allows us to approximate the total cross section via

$$\sigma \approx \frac{\omega_{\text{out}}^2 L_{\parallel}^2}{4} \int d^2r_{\perp} |j_{\perp}^{\text{eff}}(\mathbf{r}_{\perp})|^2, \quad (14)$$

with the interaction length  $L_{\parallel} = \int dr_{\parallel} f(r_{\parallel})$ . Note that this total cross section (14) contains all three Bragg peaks, the main peak centered at  $\Delta\mathbf{k} = 0$  as well as the two side peaks centered at  $\Delta\mathbf{k} = \pm 2\mathbf{k}_1$ . This can be understood by Fourier decomposition of the standing wave profile  $j^{\text{eff}} \propto \cos^2(\mathbf{k}_1 \cdot \mathbf{r}) = [1 + \cos(2\mathbf{k}_1 \cdot \mathbf{r})]/2$ .

The constant term 1/2 stems from the contributions  $\mathbf{E}_1^2$  and  $\mathbf{E}_2^2$  where both optical photons belong to the same beam and results in the central peak at  $\Delta\mathbf{k} = 0$ . The oscillating term  $\propto \cos(2\mathbf{k}_1 \cdot \mathbf{r})$ , on the other hand, stems from the mixed contribution  $2\mathbf{E}_1 \cdot \mathbf{E}_2$  involving one optical

photon from each beam. This term generates the momentum transfer  $\Delta\mathbf{k} = \pm 2\mathbf{k}_1$  and results in the side peaks. Hence, each side peak has roughly half the amplitude of the main peak at  $\Delta\mathbf{k} = 0$ .

Focusing on the experimentally most relevant side peaks at  $\Delta\mathbf{k} = \pm 2\mathbf{k}_1$ , we find the total cross section for the case  $\mathbf{e}_{\text{in}} = \mathbf{e}_{\text{out}} = \mathbf{e}_1$  after spatial and temporal average to be  $\sigma_{\pm} \approx 4\omega_{\text{out}}^2 L_{\parallel}^2 A_{\perp} a^2 E_1^4$  for each side peak, where  $A_{\perp}$  is the effective focus area seen by the XFEL. Roughly speaking, the ratio  $\sigma_{\pm}/A_{\perp}$  determines the probability that an XFEL photon hitting the optical laser focus will get scattered. Inserting the QED value for  $a$ , we find

$$\sigma_{\pm} \approx 4A_{\perp} \left( \omega_{\text{out}} L_{\parallel} \frac{\alpha_{\text{QED}} E_1^2}{90\pi E_{\text{crit}}^2} \right)^2, \quad (15)$$

where  $\alpha_{\text{QED}} \approx 1/137$  is the fine structure constant.

For the XFEL polarization  $\mathbf{e}_{\text{in}} = \mathbf{e}_{\text{out}} = \pm\mathbf{n}_1$  along the other major axis of the refractive index [52], the magnetic field of the XFEL interacts with the electric field of the optical laser via the  $b$  term in Eq. (1). Inserting the QED prediction  $b = 7a$ , the signal would be a factor of  $(7/4)^2 \approx 3$  higher, but otherwise the same conclusions as above apply. Furthermore, this channel would also be sensitive to potential axion or axionlike particles.

## VI. “FIVE O’CLOCK” SCENARIO

As a scenario where the final x-ray photon does also receive an energy shift, we consider the superposition of two optical lasers with different frequencies, such as  $\omega_2 = 2\omega_1$  (which could be generated by frequency doubling, for example). Keeping the XFEL perpendicular to the first optical laser  $\mathbf{n}_{\text{in}} \perp \mathbf{n}_1$ , we may satisfy energy and momentum conservation by tilting the second laser by  $30^\circ$  such that  $\mathbf{n}_{\text{in}} \cdot \mathbf{n}_2 = 1/2$ . The resulting momentum transfer in the forward direction is then consistent with the energy shift  $\omega_{\text{out}} = \omega_{\text{in}} \pm \omega_1$ . To maximize the transversal momentum transfer (i.e., the scattering angle), we may choose an orientation where  $\mathbf{n}_2$  lies in the same plane as  $\mathbf{n}_1$  and  $\mathbf{n}_{\text{in}}$  but almost opposite to  $\mathbf{n}_1$ , i.e.,  $\mathbf{n}_1 \cdot \mathbf{n}_2 = -\sqrt{3}/2$ . Picturing  $\mathbf{n}_1$  as vertical and  $\mathbf{n}_{\text{in}}$  as horizontal,  $\mathbf{n}_1$  and  $\mathbf{n}_2$  look like the hands of a clock at five or seven o’clock; see Fig. 1(c).

Naturally, the angular dependence (10) of  $\mathfrak{F}$  is a bit more involved than in the previous sections, but the general behavior is quite similar. For example, if all polarizations  $\mathbf{e}_{\text{in}} = \mathbf{e}_{\text{out}} = \mathbf{e}_1 = \mathbf{e}_2$  are perpendicular to the plane spanned by  $\mathbf{n}_1$  and  $\mathbf{n}_2$ , we find that only the  $a$  term contributes  $\mathfrak{F}_{\parallel} = 2a$ , analogous to Eq. (12). As before, there is no polarization flip in this specific and highly symmetric case  $\mathbf{n}_1 \perp \mathbf{e}_{\text{in}} = \mathbf{e}_{\text{out}} = \mathbf{e}_1 = \mathbf{e}_2 \perp \mathbf{n}_2$ , but, for most other orientations, we do also obtain a birefringent signal  $\mathfrak{F}_{\perp}$ ; see Appendix A.

Note that the five o’clock scenario considered here is different from the “y scenario” studied in [40]. Although

both feature the same energy shift  $\omega_{\text{out}} = \omega_{\text{in}} \pm \omega_1$ , the five o'clock scenario offers a larger momentum transfer and, thus, scattering angle.

## VII. EXPERIMENTAL PARAMETERS

Let us discuss possible experimental realizations and estimate the order of magnitude of the expected signal, where we take the experimental capabilities at HIBEF as an example. As a high energy density instrument [64], the European XFEL is combined with the Relax laser [65] provided by the HIBEF user consortium. We start with a conservative estimate and insert values which have already been shown to be reachable experimentally. The optical laser is characterized by its frequency  $\omega_L = 1.5$  eV and focus intensity  $3.5 \times 10^{20}$  W/cm<sup>2</sup>, as well as focus width 2.5  $\mu\text{m}$  and length 9  $\mu\text{m}$  (corresponding to a duration of 30 fs) [65].

For the XFEL, we assume a frequency  $\omega_{\text{in}} = 6$  keV with  $10^{12}$  photons per pulse (corresponding to an energy of 1 mJ), focused to a width between 4 and 5  $\mu\text{m}$  with a beam divergence of 80  $\mu\text{rad}$  [64]. A tighter focus is possible with a different lensing system (e.g., the CRL4 lens [64]), but then the beam divergence would increase by an order of magnitude.

However, in view of the scattering angle of 500  $\mu\text{rad}$  (for  $\omega_L = 1.5$  eV and  $\omega_{\text{in}} = 6$  keV) for the crossed-beam scenario, it is probably better to employ the lower beam divergence (or use more involved schemes, such as the dark-field method; see, e.g., [53]). Placing the detector at a distance of 7 m to the interaction point, the scattering angle of 500  $\mu\text{rad}$  yields a deflection by 3.5 mm which is expected to be sufficient for discriminating the scattered signal from the XFEL beam. For example, for the idealized case of a Gaussian beam with a beam divergence of 80  $\mu\text{rad}$ , the number of photons outside an angle of 400  $\mu\text{rad}$  is already suppressed by more than 20 orders of magnitude (for 500  $\mu\text{rad}$  more than 30).

Now we are in the position to provide a rough estimate of the number of scattered photons in such an experiment. As already explained in Sec. VB, the finite size of the optical laser focus leads to a cutoff for the spatial integral in the amplitude (7) in terms of the effective focus volume  $V_{\text{eff}}$ . Thus, the differential cross section scales as (up to dimensionless kinematical factors like  $\mathfrak{F}_a$  and  $\mathfrak{F}_b$  as well as spatial and temporal overlap integrals)

$$\frac{d\sigma}{d\Omega} = \mathcal{O}\left(\frac{\alpha_{\text{QED}}^2}{(360\pi^2)^2} \frac{E_L^4}{E_{\text{crit}}^4} \omega_{\text{in}}^4 V_{\text{eff}}^2\right). \quad (16)$$

Inserting the values above, this differential cross section becomes  $d\sigma/d\Omega = \mathcal{O}(10^{-8} \mu\text{m}^2)$ . However, as also explained in Sec. VB, this value is valid only in a comparably small solid angle of  $\Delta\Omega = \mathcal{O}(10^{-9})$  corresponding to the size of the diffraction peak, which is

determined by the spatial extent of the optical laser focus [66]. Thus, the total cross section for this Bragg peak reads  $\sigma = \mathcal{O}(10^{-17} \mu\text{m}^2)$ , which corresponds to Eq. (15).

As a result, one obtains  $\mathcal{O}(10^{-6})$  signal photons per shot or one signal photon per  $\mathcal{O}(10^6)$  shots. Even with a repetition rate of 5 Hz,  $10^6$  shots correspond to more than two days of continuous measurements. While not impossible, such an experiment would certainly be extremely challenging. The smallness of the signal again demonstrates the paramount importance of suppressing the background as much as possible.

Thus, let us discuss options to enhance the signal. The most obvious possibility is to increase the optical laser intensity, since the signal scales with the square of that quantity. An intensity of  $10^{21}$  W/cm<sup>2</sup> is already technically available and shall be provided in the near future. This would enhance the signal by one order of magnitude. Further upgrades should enable us to reach  $10^{22}$  W/cm<sup>2</sup>, yielding another increase of the signal by 2 additional orders of magnitude.

In principle, increasing the XFEL frequency (to 12 keV, for example) also enhances the cross section but, on the other hand, reduces the scattering angle (if the optical laser frequency is kept constant) and typically lowers the number of XFEL photons. Thus, balancing the advantages and drawbacks should determine the optimum XFEL frequency. Of course, increasing the number of XFEL photons (with all other relevant quantities staying the same) would be advantageous. Similarly, a larger volume  $V_{\text{eff}}$  of the optical laser focus, as long as it is not at the expense of the intensity, would increase the scattering yield.

One way to realize the collision of the two optical pulses could be the setup already proposed in [31], for example, where each laser pulse, after the collision at the focus, hits the parabolic mirror used to focus the other laser pulse—and, thus, retraces its optical path. In this scenario, the two laser pulses are basically the time reversals of each other, which requires some fine-tuning of the optical paths. A way to avoid this fine-tuning and potential damage is to tilt both optical axes a bit [corresponding to a “five-past-five” geometry; see Fig. 1(d)] such that the optical paths of the two pulses overlap only at the focus. This five-past-five geometry would reduce the momentum transfer and, thus, scattering angle a bit but might be easier to realize experimentally.

Developing this idea further, one could also imagine tilting the optical axes even more, e.g., in the form of a “ten-past-four” geometry; see Fig. 1(e). In this way, one could interpolate between the crossed-beam case in Sec. V and the counterpropagating scenario in Sec. IV. Going from the crossed-beam to the counterpropagating case has two main advantages. First, the amplitude increases; compare Eqs. (11) and (12) and Appendix A. Second, the interacting length is enlarged. Both would enhance the signal strength. As a drawback, the momentum transfer

and, thus, scattering angle is reduced. Hence, an optimum tilt angle is determined by the trade-off between signal strength and background suppression (as well as experimental constraints).

As in many of the other proposals for detecting vacuum birefringence, the polarization of the x-ray photons can be distinguished via Bragg reflection crystals. Those can be designed to also provide the energy resolution which would allow us to detect the energy shift in the five-o'clock scenario. The required frequency doubling of one of the laser pulses could be achieved with nonlinear crystals. So far, this process has been demonstrated with an efficiency above 10%, which should be increased in the future. Having achieved a sufficient efficiency (or initial laser power), one could also imagine realizing the crossed-beam scenario with two frequency-doubled pulses, which would imply doubling the momentum transfer and, thus, scattering angle.

### VIII. CONCLUSIONS

As an example of light-by-light scattering, we study the interaction of x-ray photons with ultrastrong optical lasers and compare different scenarios. Apart from the counter-propagating case already discussed in the literature, we consider the crossed-beam case and the five-o'clock scenario, as well as interpolating cases such as the five-past-five and the ten-past-four scenarios; see Fig. 1. All cases yield scattering amplitudes of comparable order of magnitude, facilitate birefringent scattering, and allow us to address the  $a$  and  $b$  parameters in the effective Euler-Heisenberg Lagrangian separately via adjusting the polarization vectors accordingly.

As a difference, the interaction length is set by the pulse length of the optical laser focus in the first (counter-propagating) case, while it is mainly determined by the focal width in the crossed-beam case (and accordingly for the other scenarios). More important, however, is the distinction between the initial and final x-ray photons, which allows us to discriminate them from the background. In the first (counter-propagating) case, the only measurable difference is their polarization—at least in the plane-wave approximation. A finite scattering angle (corresponding to a nonzero momentum transfer) can be induced only by the spatial inhomogeneity of the laser focus, which makes it a comparably small effect; see also [48]. In contrast, the other scenarios lead to a significantly larger momentum transfer. For example, taking an optical laser with  $\omega_1 = 1.5$  eV and an XFEL with 6 keV, we find scattering angles of around half a millirad, which helps us to separate the signal photons from the background (i.e., the main XFEL beam).

Furthermore, the five-o'clock scenario—while a bit more challenging to set up experimentally—would also yield an energy shift (of 1.5 eV in our example) of the final photons, which provides yet another important channel for separating signal and background. These findings motivate further

studies and give rise to the hope for observing this fundamental QED phenomenon at experimental facilities such as HIBEF.

Our results are based on the lowest-order Euler-Heisenberg Lagrangian in combination with scattering theory. This approach is justified because all involved fields, i.e., the optical laser and the XFEL, are well below the Schwinger critical fields  $E_{\text{crit}}$  and  $B_{\text{crit}}$  while all involved frequencies and momenta are well below the electron mass; see also [67–70]. In this limit, our results coincide with the locally constant field approximation; see, e.g., [71]. Note, however, that one should not employ the locally constant field approximation on the level of ray optics—because this would not reproduce the diffraction properties (Bragg peaks) which are important for the scattering angle—but on the level of wave optics.

There are several ways to go beyond this lowest-order approach. If the optical laser fields are even stronger (approaching the Schwinger critical fields) while the XFEL fields remain much smaller, we may still employ scattering theory but now based on the full Euler-Heisenberg Lagrangian (including higher-order terms in the field strengths). For higher frequency and momentum scales, the situation becomes more difficult. One way could be to include higher-order derivative terms in the Euler-Heisenberg Lagrangian or to employ the worldline representation [72,73]. For the special case of plane-wave fields, one can employ the well-known Volkov solutions; see, e.g., [69,70]. Note, however, that such plane-wave fields (which approach the constant-crossed-field case for slowly varying fields) describe the counterpropagating case (a) in Fig. 1 but not the other cases (b)–(e).

### ACKNOWLEDGMENTS

The authors acknowledge fruitful discussions with H. Gies, F. Karbstein, and R. Sauerbrey as well as funding by the Deutsche Forschungsgemeinschaft (DFG, German Research Foundation)—Project-ID No. 278162697—SFB 1242.

### APPENDIX A: PLANAR CONFIGURATION

In this section, we present a formula for the most general planar case where all the wave vectors (momenta) of the pump as well as the probe laser lie on a plane, which for simplicity can be taken to be the  $xy$  plane. We further express

$$\begin{aligned} \mathbf{n}_1 &\rightarrow \cos \theta_1 \mathbf{e}_x + \sin \theta_1 \mathbf{e}_y, & \mathbf{n}_{\text{in}} &\rightarrow \mathbf{e}_y, \\ \mathbf{n}_2 &\rightarrow \cos \theta_2 \mathbf{e}_x + \sin \theta_2 \mathbf{e}_y, & \omega_2 &= l\omega_1, \end{aligned} \quad (\text{A1})$$

where  $\theta_i$  is the angle that the unit vector  $\mathbf{n}_i$  makes with the  $x$  axis while  $l > 0$  denotes the ratio of the two optical laser frequencies. Up to the order of  $\mathcal{O}(\omega_{\text{in}}^{-1})$ , the following relation is, thus, to be satisfied if one desires to stay in the kinematically allowed region:

$$\sin \theta_2 = \frac{\sin \theta_1 + l - 1}{l}. \quad (\text{A2})$$

We choose the following parametrization of the laser's and XFEL's polarizations:

$$\begin{aligned} \mathbf{e}_1 &= (\sin \alpha_1 \sin \theta_1, -\sin \alpha_1 \cos \theta_1, \cos \alpha_1), \\ \mathbf{e}_2 &= (-\sin \alpha_2 \sin \theta_2, \sin \alpha_2 \cos \theta_2, \cos \alpha_2), \\ \mathbf{e}_{\text{in}} &= (\sin \alpha_{\text{in}}, 0, \cos \alpha_{\text{in}}), \\ \mathbf{e}_{\text{out}} &= (\sin \alpha_{\text{out}}, 0, \cos \alpha_{\text{out}}), \end{aligned} \quad (\text{A3})$$

where  $\alpha_i$  ( $i = 1, 2, \text{in}, \text{out}$ ) is the angle formed by the polarization vector  $\mathbf{e}_i$  with respect to  $\mathbf{e}_z$ . Inserting this parametrization into Eqs. (9) and (10) and summing over the permutations, the function  $\mathfrak{F}$  in this fully planar scenario is finally given by

$$\begin{aligned} \mathfrak{F} &= \frac{1}{2}(1 - \sin \theta_1)(1 - \sin \theta_2) \\ &\times [(4a + b) \cos(\alpha_1 + \alpha_2) \cos(\alpha_{\text{in}} - \alpha_{\text{out}}) \\ &+ (4a - b) \cos(\alpha_1 - \alpha_2 + \alpha_{\text{in}} + \alpha_{\text{out}})]. \end{aligned} \quad (\text{A4})$$

For the birefringent case  $\mathbf{e}_{\text{in}} \perp \mathbf{e}_{\text{out}}$ , the angles satisfy  $\alpha_{\text{in}} - \alpha_{\text{out}} = \pm\pi/2$ , and, thus, only the term  $\propto (4a - b)$  in the last line survives [52]. Recall that  $\theta_2$  is fixed by Eq. (A2) if one desires to obtain a nonvanishing amplitude.

## APPENDIX B: EXPLICIT EXPRESSIONS FOR THE CURRENTS

The explicit expression for the effective source in Eq. (5) is

$$\begin{aligned} \mathbf{J}^{\text{eff}} &= \nabla \times \{ \nabla \times [\delta\epsilon \cdot \mathbf{E} + \delta\Psi \cdot \mathbf{B}] \} + \partial_t \{ \nabla \times [-\delta\mu \cdot \mathbf{B} - \delta\Psi^T \cdot \mathbf{E}] \} \\ &= \nabla \times \{ \nabla \times [(8aE_L^i E_L^j + 2bB_L^i B_L^j + 4a\delta^{ij}(\mathbf{E}_L^2 - \mathbf{B}_L^2))E_j + (-8aE_L^i B_L^j + 2bB_L^i E_L^j + 2b\delta^{ij}(\mathbf{E}_L \cdot \mathbf{B}_L))B_j] \} \\ &\quad + \partial_t \{ \nabla \times [-(2bE_L^i E_L^j + 8aB_L^i B_L^j - 4a\delta^{ij}(\mathbf{E}_L^2 - \mathbf{B}_L^2))B_j - (-8aE_L^j B_L^i + 2bB_L^j E_L^i + 2b\delta^{ij}(\mathbf{E}_L \cdot \mathbf{B}_L))E_j] \}, \end{aligned} \quad (\text{B1})$$

where we have employed the effective permittivity, permeability, and symmetry-breaking tensors in Eqs. (3) and (4).

In going from Eq. (5) to (6), the time Fourier transform of the effective source is needed:

$$\mathbf{J}_\omega^{\text{eff}}(t) = \int_{-\infty}^{\infty} \frac{d\omega}{(2\pi)} e^{-i\omega t} \tilde{\mathbf{J}}_\omega^{\text{eff}}. \quad (\text{B2})$$

Since we are employing the Born approximation, energy conservation implies that the only contributions are those that satisfy  $\omega_{\text{out}} = \omega_{\text{in}} \pm \omega_1 \pm \omega_2$ . Hence, we can strip the delta functions from the effective source defining

$$\tilde{\mathbf{J}}_\omega^{\text{eff}} = \sum_{\omega_{\text{out}} = \omega_{\text{in}} \pm \omega_1 \pm \omega_2} \delta(\omega - \omega_{\text{out}}) \mathbf{J}_\omega^{\text{eff}}. \quad (\text{B3})$$

An analogous definition applies to  $\mathbf{D}_\omega^{\text{out}}$ . Notice that in Eq. (6), to simplify the reading, we are writing  $\mathbf{J}_\omega$  instead of  $\mathbf{J}_{\omega_{\text{out}}}$ .

Lastly, in Eq. (13), we Fourier transform back to the time domain and afterward perform a time average:

$$\begin{aligned} j^{\text{eff}} &= \frac{1}{\omega_{\text{out}}^2 |\mathbf{D}_\omega^{\text{in}}|} e^{-i\mathbf{k}_{\text{in}} \cdot \mathbf{r}} \lim_{T \rightarrow \infty} \frac{1}{T} \int_{-T}^T dt \mathbf{e}_{\text{out}} \cdot \mathbf{J}^{\text{eff}}(t) \\ &= \frac{1}{\omega_{\text{out}}^2 |\mathbf{D}_\omega^{\text{in}}|} e^{-i\mathbf{k}_{\text{in}} \cdot \mathbf{r}} \\ &\quad \times \lim_{T \rightarrow \infty} \frac{1}{T} \int_{-T}^T dt \int_{-\infty}^{\infty} \frac{d\omega}{2\pi} e^{-i\omega t} \mathbf{e}_{\text{out}} \cdot \tilde{\mathbf{J}}_\omega^{\text{eff}}. \end{aligned} \quad (\text{B4})$$

- [1] H. Euler and B. Kockel, Über die Streuung von Licht an Licht nach der Diracschen Theorie, *Naturwissenschaften* **23**, 246 (1935).  
[2] W. Heisenberg and H. Euler, Folgerungen aus der Diracschen Theorie des Positrons, *Z. Phys.* **98**, 714 (1936).  
[3] R. Karplus and M. Neuman, The scattering of light by light, *Phys. Rev.* **83**, 776 (1951).

- [4] F. Sauter, Über das Verhalten eines Elektrons im homogenen elektrischen Feld nach der relativistischen Theorie Diracs, *Z. Phys.* **69**, 742 (1931).  
[5] J. Schwinger, On gauge invariance and vacuum polarization, *Phys. Rev.* **82**, 664 (1951).  
[6] L. Meitner and H. Kösters (with addition from M. Delbrück), Über die Streuung kurzweiliger  $\gamma$ -Strahlen, *Z. Phys.* **84**, 137 (1933).

- [7] H. A. Bethe and F. Rohrlich, Small angle scattering of light by a Coulomb field, *Phys. Rev.* **86**, 10 (1952).
- [8] V. Costantini, B. De Tollis, and G. Pistoni, Nonlinear effects in quantum electrodynamics, *Nuovo Cimento Soc. Ital. Fis. A* **2**, 733 (1971).
- [9] G. Jarlskog, L. Jönsson, S. Prünster, H. D. Schulz, H. J. Willutzki, and G. G. Winter, Measurement of Delbrück scattering and observation of photon splitting at high energies, *Phys. Rev. D* **8**, 3813 (1973).
- [10] A. I. Milstein and V. M. Strakhovneko, Quasiclassical approach to the high-energy Delbrück scattering, *Phys. Rev. A* **95**, 135 (1983).
- [11] A. I. Milstein and V. M. Strakhovneko, Coherent scattering of high-energy photons in a Coulomb field, *Sov. Phys. JETP* **58**, 8 (1983).
- [12] Sh. Zh. Akhmadaliev *et al.*, Delbrück scattering at energies of 140–450 MeV, *Phys. Rev. C* **58**, 2844 (1998).
- [13] A. I. Milstein and M. Schumacher, Present status of Delbrück scattering, *Phys. Rep.* **243**, 183 (1994).
- [14] M. Schumacher, Delbrück scattering, *Radiat. Phys. Chem.* **56**, 101 (1999).
- [15] P. Papatzacos and K. Mork, Delbrück scattering calculations, *Phys. Rev. D* **12**, 206 (1975).
- [16] P. Papatzacos and K. Mork, Delbrück scattering, *Phys. Rep.* **21**, 81 (1975).
- [17] ATLAS Collaboration, Evidence for light-by-light scattering in heavy-ion collisions with the ATLAS detector at the LHC, *Nat. Phys.* **13**, 852 (2017).
- [18] D. d’Enterria and G. G. da Silveira, Observing Light-by-Light Scattering at the Large Hadron Collider, *Phys. Rev. Lett.* **111**, 080405 (2013).
- [19] N. Ahmadianiaz, M. Bussmann, T. E. Cowan, A. Debus, T. Kluge, and R. Schützhold, Observability of Coulomb-assisted quantum vacuum birefringence, *Phys. Rev. D* **104**, L011902 (2021).
- [20] D. Valle, A. Ejlli, U. Gastaldi, G. Messineo, E. Milotti, R. Pengo, G. Ruoso, and G. Zavattini, The PVLAS experiment: Measuring vacuum birefringence and dichroism with a birefringent Fabry Perot cavity, *Eur. Phys. J. C* **76**, 24 (2016).
- [21] E. Zavattini, U. Gastaldi, R. Pengo, G. Ruoso, F. Della Valle, and E. Milotti, Measuring the magnetic birefringence of vacuum: The PVLAS experiment, *Int. J. Mod. Phys. A* **27**, 1260017 (2012).
- [22] D. Valle, G. Di Domenico, U. Gastaldi, E. Milotti, R. Pengo, G. Ruoso, and G. Zavattini, Towards a direct measurement of vacuum magnetic birefringence: PVLAS achievements, *Opt. Commun.* **283**, 4194 (2010).
- [23] E. Zavattini *et al.*, New PVLAS results and limits on magnetically induced optical rotation and ellipticity in vacuum, *Phys. Rev. D* **77**, 032006 (2008).
- [24] E. Zavattini *et al.*, Experimental Observation of Optical Rotation Generated in Vacuum by a Magnetic Field, *Phys. Rev. Lett.* **96**, 110406 (2006).
- [25] A. Ejlli, F. Della Valle, U. Gastaldi, G. Messineo, R. Pengo, G. Ruoso, and G. Zavattini, The PVLAS experiment: A 25 year effort to measure vacuum magnetic birefringence, *Phys. Rep.* **871**, 1 (2020).
- [26] X. Fan *et al.*, The OVAL experiment: A new experiment to measure vacuum magnetic birefringence using high repetition pulsed magnets, *Eur. Phys. J. D* **71**, 308 (2017).
- [27] M. T. Hartman, R. Battesti, and C. Rizzo, Characterization of the vacuum birefringence polarimeter at BMV: Dynamical cavity mirror birefringence, *IEEE Trans. Instrum. Meas.* **68**, 2268 (2019).
- [28] M. T. Hartman, A. Rivère, R. Battesti, and C. Rizzo, Noise characterization for resonantly-enhanced polarimetric vacuum magnetic-birefringence experiments, *Rev. Sci. Instrum.* **88**, 123114 (2017).
- [29] R. Battesti *et al.*, High magnetic fields for fundamental physics, *Phys. Rep.* **765**, 1 (2018).
- [30] N. Ahmadianiaz, T. E. Cowan, R. Sauerbrey, U. Schramm, H.-P. Schlenvoigt, and R. Schützhold, On the Heisenberg limit for detecting vacuum birefringence, *Phys. Rev. D* **101**, 116019 (2020).
- [31] T. Heinzl, B. Liesfeld, K.-U. Amthor, H. Schwöerer, R. Sauerbrey, and A. Wipf, On the observation of vacuum birefringence, *Opt. Commun.* **267**, 318 (2006).
- [32] A. Di Piazza, K. Z. Hatsagortsyan, and C. H. Keitel, Light Diffraction by a Strong Standing Electromagnetic Wave, *Phys. Rev. Lett.* **97**, 083603 (2006).
- [33] T. Inada *et al.*, Search for photon-photon elastic scattering in the x-ray region, *Phys. Lett. B* **732**, 356 (2014).
- [34] T. Yamaji *et al.*, An experiment of x-ray photon-photon elastic scattering with a Laue-case beam collider, *Phys. Lett. B* **763**, 454 (2016).
- [35] H.-P. Schlenvoigt, T. Heinzl, U. Schramm, T. Cowan, and R. Sauerbrey, Detecting vacuum birefringence with X-ray free electron lasers and high-power optical lasers: A feasibility study, *Phys. Scr.* **91**, 023010 (2016).
- [36] F. Karbstein and C. Sundqvist, Probing vacuum birefringence using x-ray free electron and optical high-intensity lasers, *Phys. Rev. D* **94**, 013004 (2016).
- [37] E. Lundström, G. Brodin, J. Lundin, M. Marklund, R. Bingham, J. Collier, J. T. Mendonça, and P. Norreys, Using High-Power Laser for Detection of Elastic Photon-Photon Scattering, *Phys. Rev. Lett.* **96**, 083602 (2006).
- [38] T. Inada, T. Yamazaki, T. Yamaji, Y. Seino, X. Fan, S. Kamioka, T. Namba, and S. Asai, Probing physics in vacuum using an x-ray free-electron laser, a high-power laser, and a high-field magnet, *Appl. Sci.* **7**, 671 (2017).
- [39] A. Di Piazza, A. I. Milstein, and C. H. Keitel, Photon splitting in a laser field, *Phys. Rev. A* **76**, 032103 (2007).
- [40] B. King, H. Hu, and B. Shen, Three-pulse photon-photon scattering, *Phys. Rev. A* **98**, 023817 (2018).
- [41] D. Tommasini, A. Ferrando, H. Michinel, and M. Seco, Precision tests of QED and non-standard models by searching photon-photon scattering in vacuum with high power lasers, *J. High Energy Phys.* **11** (2009) 043.
- [42] D. Tommasini and H. Michinel, Light by light diffraction in vacuum, *Phys. Rev. A* **82**, 011803 (2010).
- [43] B. King and Ch. Keitel, Photon-photon scattering in collisions of intense laser pulses, *New J. Phys.* **14**, 103002 (2012).
- [44] H. Gies, F. Karbstein, and N. Seegert, Quantum reflection as a new signature of quantum vacuum nonlinearity, *New J. Phys.* **15**, 083002 (2013).
- [45] H. Gies, F. Karbstein, and C. Kohlfürst, Photon-photon scattering at the high-intensity frontier, *Phys. Rev. D* **97**, 076002 (2018).

- [46] H. Gies, F. Karbstein, and C. Kohlfürst, All-optical signatures of strong-field QED in the vacuum emission picture, *Phys. Rev. D* **97**, 036022 (2018).
- [47] B. Döbrich and H. Gies, Interferometry of light propagation in pulsed fields, *Europhys. Lett.* **87**, 21002 (2009).
- [48] H. Gies, F. Karbstein, and N. Seegert, Quantum reflection of photons off spatio-temporal electromagnetic field inhomogeneities, *New J. Phys.* **17**, 043060 (2015).
- [49] H. Grote, On the possibility of vacuum QED measurements with gravitational wave detectors, *Phys. Rev. D* **91**, 022002 (2015).
- [50] H. Gies, F. Karbstein, and L. Klar, All-optical quantum vacuum signals in two-beam collision, *Phys. Rev. D* **106**, 116005 (2022).
- [51] F. Karbstein, C. Sundqvist, K. S. Schulze, I. Uschmann, H. Gies, and G. G. Paulus, Vacuum birefringence at x-ray free-electron lasers, *New J. Phys.* **23**, 095001 (2021).
- [52] In a calcite crystal, birefringence can manifest itself as a doubly refracted image of the same object, caused by the different refractive indexes of the two polarizations. Apart from such a double image, the difference in the refractive indexes can also induce a relative phase shift between the photon amplitudes of the two polarizations. If the incident photon polarization is not oriented along the major axes of the index of refraction, this phase shift will induce a rotation in polarization—which is the signal considered here.
- [53] F. Karbstein, D. Ullmann, E. A. Mosman, and M. Zepf, Direct Accessibility of the Fundamental Constants Governing Light-by-Light Scattering, *Phys. Rev. Lett.* **129**, 061802 (2022).
- [54] F. Karbstein, Probing vacuum polarization effects with high-intensity lasers, *Particles* **3**, 39 (2020).
- [55] B. King and T. Heinzl, Measuring vacuum polarisation with high power lasers, *High Power Laser Sci. Eng.* **4** (2016).
- [56] A. Di Piazza, C. Müller, K. Z. Hatsagortsyan, and C. H. Keitel, Extremely high-intensity laser interactions with fundamental quantum systems, *Rev. Mod. Phys.* **84**, 1177 (2012).
- [57] G. V. Dunne, The Heisenberg-Euler effective action: 75 years on, *Int. J. Mod. Phys. A* **27**, 1260004 (2012).
- [58] J. S. Toll, The dispersion relation for light and its application to problems involving electron pairs, Ph.D. thesis, Princeton University, Princeton, NJ, USA, 1952.
- [59] P. Sikivie, D. B. Tanner, and K. van Bibber, Resonantly Enhanced Axion-Photon Regeneration, *Phys. Rev. Lett.* **98**, 172002 (2007).
- [60] P. Sikivie, Experimental Tests of the “Invisible” Axion, *Phys. Rev. Lett.* **51**, 1415 (1984).
- [61] G. Raffelt and L. Stodolsky, Mixing of the photon with low-mass particles, *Phys. Rev. D* **37**, 1237 (1988).
- [62] P. A. Zyla *et al.* (Particle Data Group), Axions and other similar particles, *Prog. Theor. Exp. Phys.* **2020**, 083C01 (2020).
- [63] J. D. Jackson, *Classical Electrodynamics* (John Wiley & Sons, New York, 2007).
- [64] U. Zastra *et al.*, The high energy density scientific instrument at the European XFEL, *J. Synchrotron Radiat.* **28**, 1393 (2021).
- [65] A. Laso Garcia *et al.*, ReLaX: The Helmholtz International Beamline for Extreme Fields high-intensity short-pulse laser driver for relativistic laser-matter interaction and strong-field science using the high energy density instrument at the European x-ray free electron laser facility, *High Power Laser Sci. Eng.* **9**, E59 (2021).
- [66] Taking into account the space-time distribution of the optical laser focus (modeled as a Gaussian beam) as well as the associated energy and momentum spread, the variations of the scattering angle (i.e., the size of the Bragg peak) are below 90  $\mu$ rad, i.e., comparable to the initial beam divergence.
- [67] I. A. Aleksandrov and V. M. Shabaev, Vacuum birefringence and dichroism in a strong plane-wave background, [arXiv:2303.16273](https://arxiv.org/abs/2303.16273).
- [68] I. A. Aleksandrov, G. Plunien, and V. M. Shabaev, Photon emission in strong fields beyond the locally-constant field approximation, *Phys. Rev. D* **100**, 116003 (2019).
- [69] S. Bargin, S. Meuren, C. H. Keitel, and A. Di Piazza, High-Energy Vacuum Birefringence and Dichroism in an Ultrastrong Laser Field, *Phys. Rev. Lett.* **119**, 250403 (2017).
- [70] S. Meuren, C. H. Keitel, and A. Di Piazza, Polarization operator for plane-wave background fields, *Phys. Rev. D* **88**, 013007 (2013).
- [71] F. Karbstein and R. Shaisultanov, Photon propagation in slowly varying inhomogeneous fields, *Phys. Rev. D* **91**, 085027 (2015).
- [72] N. Ahmadinia, C. Lopez-Arcos, M. A. Lopez-Lopez, and C. Schubert, The QED four-photon amplitudes off-shell: Part 1, *Nucl. Phys.* **B991**, 116216 (2023).
- [73] N. Ahmadinia, C. Lopez-Arcos, M. A. Lopez-Lopez, and C. Schubert, The QED four-photon amplitudes off-shell: Part 2, *Nucl. Phys.* **B991**, 116217 (2023).